The Spindle Pole Body Assembly Component Mps3p/Nep98p Functions in Sister Chromatid Cohesion*

Lisa M. Antoniacci‡, Margaret A. Kenna‡, Peter Uetz§¶, Stanley Fields§‖, and Robert V. Skibbens‡**

From the ‡Department of Biological Sciences, Lehigh University, Bethlehem, Pennsylvania 18015, §Departments of Genome Sciences and Medicine, University of Washington, Seattle, Washington 98195, and the ‖Departments of Genetics and Medicine, Howard Hughes Medical Institute, University of Washington, Seattle, Washington 98195-7360

For successful chromosome segregation during mitosis, several processes must occur early in the cell cycle, including spindle pole duplication, DNA replication, and the establishment of cohesion between nascent sister chromatids. Spindle pole body duplication begins in G_1 and continues during early S-phase as spindle pole bodies mature and start to separate. Key steps in spindle pole body duplication are the sequential recruitment of Cdc31p and Spc42p by the nuclear envelope transmembrane protein Msp3p/Nep98p (herein termed Mps3p). Concurrent with DNA replication, Ctf7p/Eco1p (herein termed Ctf7p) ensures that nascent sister chromatids are paired together, identifying the products of replication as sister chromatids. Here, we provide the first evidence that the nuclear envelope spindle pole body assembly component Mps3p performs a function critical to sister chromatid cohesion. Mps3p was identified as interacting with Ctf7p from a genome-wide two-hybrid screen, and the physical interaction was confirmed by both *in vivo* (co-immunoprecipitation) and *in vitro* (GST pull-down) assays. An *in vivo* cohesion assay on new *mps3/nep98* alleles revealed that loss of Mps3p results in precocious sister chromatid separation and that Mps3p functions after G_1, coincident with Ctf7p. Mps3p is not required for cohesion during mitosis, revealing that Mps3p functions in cohesion establishment and not maintenance. Mutated Mps3p that results in cohesion defects no longer binds to Ctf7p *in vitro*, demonstrating that the interaction between Mps3p and Ctf7p is physiologically relevant. In support of this model, *mps3 ctf7* double mutant cells exhibit conditional synthetic lethality. These findings document a new role for Mps3p in sister chromatid cohesion and provide novel insights into the mechanism by which a spindle pole body component, when mutated, contributes to aneuploidy.

Microtubule-organizing center duplication, separation, and microtubule nucleation are all essential facets of proper chromosome segregation. In budding yeast, microtubule-organizing centers, called spindle pole bodies, function on both sides of the nuclear envelope to nucleate microtubules in both the cytoplasmic and nuclear volumes. Spindle pole body duplication is a multistep process that includes formation of a satellite, expansion into a cytoplasmic duplication plaque, half-bridge growth, and subsequent insertion into the nuclear envelope (1, 2). Evidence from genetic and electron microscopy studies indicates that spindle pole body duplication starts in G_1 and continues into early S-phase. Mps3p/Nep98p (herein termed Mps3p) is an essential nuclear envelope protein that is concentrated at the nuclear envelope half-bridge and required for spindle pole body assembly. Early in spindle pole body assembly, Mps3p functions to recruit and anchor Cdc31p to the half-bridge. Later, Mps3p is required for integration of Spc42p into the spindle pole duplication plaque (3, 4).

Coincident with the latter portion of spindle pole body maturation and separation are the processes of DNA replication and cohesion establishment (2, 5). During S-phase, each chromosome replicates to produce two identical sister chromatids. To identify the products of DNA replication as sister chromatids, sisters become paired along their entire length. The initial pairing process, or cohesion establishment, ensures that cohesion occurs exclusively between sister chromatids while precluding the pairing of nonsister chromatids, homologous chromosomes, or highly repetitive DNA sequences (6–8).

Whereas the molecular mechanism by which cohesion is established remains unknown, it is clear that establishment is intimately coupled to DNA replication. Previously, we reported that the cohesion establishment factor *CTF7/ECO1* (herein termed *CTF*7) genetically interacts with both *POL30* (proliferating cell nuclear antigen) and *CHL12/CTF18* (an RFC homolog) (9). Several DNA replication factors now have been identified as functioning in cohesion, including replication factor C subunits, DNA helicases, and DNA polymerases (9–16). These findings have popularized a model in which cohesion is established as nascent sister chromatids emerge from behind the DNA replication fork (8, 17, 18). Recent findings that DNA helicases are required for sister chromatid cohesion (16, 19, 20) suggest that DNA helicases first encounter and possibly unwind DNA loci marked by cohesins. This model is supported by numerous observations that at least a subset of cohesins are associated with DNA after anaphase onset and prior to S-phase (21–23), suggesting that a cohesin subset remains from the previous cell cycle to mark loci destined for cohesion assembly reactions in the subsequent cell cycle (8, 16). Intriguingly, DNA helicases, such as budding yeast Chl1p and Sgs1p, are homologs of human factors (BACH1, Blooms, and Werners) implicated in genome maintenance, aging, and cancer progression (16, 24–27).

Here, we report on new findings that a nuclear envelope

¶ Present address: Institut fur Genetik, Forschungszentrum Karlsruhe, Germany.
** To whom correspondence should be addressed. Tel.: 610-758-6162; E-mail: rvs3@Lehigh.edu.

protein required for spindle pole body assembly also functions in sister chromatid cohesion. Several independent lines of evidence reveal that Mps3p physically associates with Ctf7p, a cohesion establishment factor. New *mps3* alleles were generated and used to show that Mps3p indeed functions in cohesion and that this activity occurs after the G_1 portion of the cell cycle. These findings reveal that a spindle pole body assembly factor performs a function that is critical to sister chromatid cohesion and proper chromosome segregation.

EXPERIMENTAL PROCEDURES

Two-hybrid Assays—pJL59 containing *CEN*, *TRP1*, and *GAL4* DNA-binding domain (BD) sequences was obtained by digesting pPC62 (*CEN*, *LEU2*, and *GAL4(BD)* and replacing the CEN-LEU2 cassette for a CEN-TRP1 cassette obtained by PvuI digestion of pRS315 (a generous gift from John Lamb) (28). pJL59 was linearized with ClaI and ligated in the presence of *CTF7* obtained by BstBI digestion of pBS2 (9). *CTF7* inserted in the reverse orientation was also obtained. Two-hybrid analyses were performed as described (29). Proper functioning of Gal4(BD)-Ctf7p was confirmed by transformation into a *ctf7* deletion strain containing (pRS316-*CTF7*). All transformants remained viable on medium supplemented with 5′-FOA[1] to counterselect for the pRS316-based plasmid (30). In contrast, transformants harboring either Gal4(BD) vector alone or vector with *CTF7* placed in the reverse orientation were inviable upon 5′-FOA exposure.

GST Pull-downs—GST-CTF7 expression in *Escherichia coli* cells was performed as previously described (14). Briefly, yeast cells containing Mps3-13MYCp, Mps3Δ60-13MYC, or Mps3-3-13MYCp were spheroplasted in 100T Zymolyase (Seikagaku), lysed by swelling and mechanical disruption (20 mM HEPES-HCl (pH 7.5), 5 mM $MgCl_2$, and protease inhibitors), and centrifuged at 9500 rpm for 45 min (model JA-20; Beckman). The supernatant was removed, and the insoluble chromatin pellet was extracted with lysis buffer containing 1 M NaCl before recentrifugation. The salt-extracted supernatant was then harvested and divided into four equal aliquots, one of which was precipitated with tricholoroaceticic acid and then resuspended in Laemmli buffer. The other three aliquots were each diluted 10-fold in lysis buffer (to reduce the salt concentration) prior to incubation with one of the three bead matrices (glutathione-Sepharose beads or beads coupled to GST or GST-Ctf7p). Incubations were performed at either 4 °C for 2 h or 37 °C for 30 min. The treated beads were washed several times before bound proteins were removed using SDS-containing solubilization buffer. During Western blot analyses, the MYC epitope was visualized using monoclonal anti-c-MYC 9E10 antibody (Santa Cruz Biotechnology, Inc., Santa Cruz, CA), goat anti-mouse horseradish peroxidase (Bio-Rad), and ECL-*Plus* (Amersham Biosciences).

Co-immunoprecipitation—Cells containing Mps3-MYCp were transformed with either Ctf7-HAp or HA only vector control 2-μm plasmids. Transformed cells were grown to log phase and then lysed with glass beads. The lysate was centrifuged, and the resulting pellet was treated with lysis buffer supplemented to 1 M NaCl and centrifuged, and the resulting salt-extracted supernatant was harvested for immunoprecipitation. Co-immunoprecipitation was performed as previously described (14) with minor modifications. Briefly, supernatants were diluted in Buffer A (50 mM Tris (pH 7.5), 50 mM NaCl, 0.2% Triton X-100) supplemented with protease inhibitors (Roche Molecular Biochemicals), incubated with A-14 polyclonal anti-MYC (Santa Cruz Biotechnology) at 4 °C, and then incubated with Protein A-Sepharose CL-4B beads (Amersham Biosciences) at 4 °C overnight. A parallel sample was also treated with Protein A-Sepharose beads without anti-MYC antibody. In both cases, beads were washed with Buffer A several times using low speed centrifugation, and bound proteins were eluted with SDS solubilization buffer. Western blot analysis was carried out using Y-11 monoclonal anti-HA antibody (Santa Cruz Biotechnology) followed by goat anti-mouse horseradish peroxidase (Bio-Rad), and ECL-*Plus* (Amersham Biosciences).

Generation of mps3 Mutant Alleles—PCR mutagenesis was performed using pSJ140 (pRS316-*MPS3*; generously provided by Drs. S. Jaspersen and M. Winey) as DNA template and limiting amounts of dNTPs as previously described (9, 31). NcoI and NdeI were used to release a 1.9-kbp fragment from pRS315-*MPS3*. The remaining vector and PCR product were then co-transformed into a yeast strain contain-

ing an *MPS3* knockout with *KAN* covered by pSJ140. Approximately 6000 transformants were plated to medium containing 5′-FOA to counterselect against pSJ140 (30). The remaining transformants (harboring potentially PCR-mutated *MPS3* as the sole source of Mps3p function) were placed on rich medium at 23 and 37 °C and scored for temperature sensitivity. From a total of six temperature-sensitive *mps3* strains identified, plasmids were recovered from the four tightest temperature-sensitive alleles. These *mps3* alleles were cloned into an integrating vector (pRS402), linearized to promote integration at the *ADE2* loci, and transformed into the *MPS3-KAN* knockout yeast strain covered by pSJ140. Transformants were then plated to medium containing 5′-FOA to counterselect against pSJ140, leaving the integrated PCR-mutagenized *mps3* alleles as the sole source of Mps3p function. Stably transfected cells were then placed on rich medium at 23 and 37 °C and scored for temperature sensitivity. All four mutants retained temperature sensitivity and were named *mps3-2*, *mps3-3*, *mps3-4*, and *mps3-5*.

Cohesion Assay—Our modified cohesion assay strain was previously described (13, 14, 32). Briefly, Tet operator repeats integrated ~40 kb from the centromere of chromosome V are detected via binding of the stably integrated GFP-Tet repressor. In addition, Pds1–13MYCp expression allows identification of preanaphase cells by immunofluorescence on a cell-by-cell basis. This cohesion assay strain was crossed with our stably integrated *mps3-3* allele strain, sporulated, and dissected. Spores harboring the appropriate markers were then assayed for cohesion defects. Log phase cells were arrested in G_1 using α factor, washed, and released into 37 °C rich medium containing nocodazole. Mitotic arrested cells were fixed and processed for immunofluorescence to visualize Pds1p (A-14 anti-MYC (Santa Cruz Biotechnology) followed by goat anti-rabbit Alexa 568 (Molecular Probes, Inc., Eugene, OR)), DNA (DAPI), and GFP. DNA content was assessed by flow cytometry using a BD Biosciences FACSCAN. For the cohesion assay performed on both α-factor and nocodazole-treated cells (Fig. 5), each 3-h data point represents >400 individual Pds1p-staining cells averaged from four independent experiments. Each 5-h data point represents 100 individual cells per strain. To test for cohesion maintenance, each data point represents 200 individual cells averaged from two independent experiments.

Spindle Pole Body Duplication Assay—Log phase wild type and *ctf7* mutant cells were placed in 23 °C rich medium supplemented with nocodazole for 3 h. The mitotic arrested cells were washed two times in 37 °C medium and allowed to proceed through the cell cycle at this temperature (restrictive for *ctf7-203*). Samples were harvested every 30 min and processed for flow cytometry and immunofluorescence. Time points in which both wild type and *ctf7* cells were judged to have traversed the cell cycle and reenter mitosis were further processed to detect Tub4p and α-tubulin (anti-Tub4p a generous gift from S. Jaspersen and M. Winey; B512 anti-α-tubulin was purchased from Sigma). Only large budded cells (bud size roughly one-half of mother) were counted. Cells in which Tub4p was not detected were also not counted. Results shown represent averages for three independent time courses in which at least 50 cells were counted for each time point.

RESULTS

Genome-wide Two-hybrid Screen Identifies Mps3p as Associating with Ctf7p—Ctf7p is an essential yeast protein that functions to establish cohesion between sister chromatids (9, 21). To identify novel cohesion establishment factors, we performed a genome-wide two-hybrid screen. The *CTF7* open reading frame (encoding for amino acids 26–281) was fused in-frame 3′ to the *GAL4* DNA binding domain (BD) sequence (28). When expressed as the sole source of Ctf7p function in yeast, Gal4(BD)-Ctf7p rescues *ctf7Δ* strain viability. These results indicate that the Gal4(BD)-Ctf7p chimera is functional *in vivo* and further reveals that amino acids 1–25 are not essential for Ctf7p function. Prior to performing the two-hybrid screen, we determined that Gal4(BD)-Ctf7p did not promote expression of any of the three reporter genes (*HIS3*, *ADE2*, and *lacZ*) utilized in the two-hybrid assay (28). Nor did Gal4(BD)-Ctf7p activate reporter gene expression in the presence of a Gal4 activation domain (AD) vector.

Yeast matings were used to introduce the *GAL4(BD)-CTF7* construct into strains that harbor a genome-wide array of full-length open reading frame sequences fused to *GAL4(AD)* (29). Expressed AD-gene fusions that interact with GAL4(BD)-Ctf7p

---

[1] The abbreviations used are: 5′-FOA, 5′-fluoroorotic acid; GST, glutathione *S*-transferase; DAPI, 4′,6-diamidino-2-phenylindole; HA, hemagglutinin; BD, binding domain; AD, activation domain.

induce *HIS3* expression, promoting growth on the appropriate selection plates. From this genome-wide screen, only two gene products exhibited strong interactions with Ctf7p. At the time that the screen was performed, one of these candidate interacting gene products was listed as an unidentified open reading frame (YJL019W). More recently, YJL019W was characterized as *MPS3*, a gene that encodes for an essential nuclear envelope spindle pole body assembly component. Defects in *MPS3* result in a monopolar spindle phenotype (3, 4). Investigations into the candidate second interactor are currently under way.

Mps3p Associates with Ctf7p under in Vitro Assembly Conditions—It became important to independently test for a physical interaction between Mps3p and Ctf7p. We first employed a GST pull-down strategy to test for a physical association *in vitro*. One advantage of GST-based purification is that physical interactions are successfully detected even for Ctf7p, which occurs *in vivo* at very low copy (14). In addition, GST pull-downs test for proteins that are competent to associate in the absence of *in vivo* assembly reactions. The entire *CTF7* open reading frame was inserted in-frame 3′ to the *GST* DNA sequence to produce *GST-CTF7* (14). Gst-Ctf7p is readily expressed in bacteria and retains functional activity *in vitro* (16, 33). We then obtained a yeast strain in which the sole source of Mps3p function is derived from *MPS3-13MYC* stably integrated into the genome (a generous gift from Drs. S. Jaspersen and M. Winey). Extracts from this stable integrated cell line contained a protein band of the appropriate molecular weight detectable by Western blot. A similar protein band was not detectable in the parental nontransformed strain.

To test for protein-protein interactions, GST-Ctf7p or GST alone were bacterially expressed and coupled to glutathione-Sepharose beads. Extracts from yeast cells expressing Mps3-13MYCp were obtained as previously described (14). The resulting soluble fraction was divided into four aliquots; one aliquot was incubated with Sepharose beads, the second aliquot was incubated with beads coupled to GST, and the third aliquot was incubated with beads coupled to GST-Ctf7p. The fourth aliquot served as a marker to identify Mps3p during Western blot analyses. The three bead matrices were copiously washed before eluting bound proteins off of the bead matrices. Western blot analyses of the eluted proteins reveal that Mps3p specifically associated with GST-Ctf7p, but that Mps3p did not associate with GST or beads alone (Fig. 1). These results provide independent confirmation of the two-hybrid interaction and demonstrate that Mps3p and Ctf7p associate *in vitro*. We repeated the GST pull-down using MYC-tagged Mps3p in which the C-terminal 60 amino acids are deleted (Mps3Δ60p). Western blot analyses indicate that Mps3Δ60p specifically associates with Ctf7p (data not shown).

Mps3p Associates with Ctf7p in Vivo—To test that Mps3p associates with Ctf7p *in vivo*, we next performed co-immunoprecipitations in which epitope-tagged Ctf7p and Mps3p were co-expressed in yeast cells. To circumvent detection problems associated with low expression levels, we used a Ctf7-HAp construct that expresses Ctf7p at elevated levels. Importantly, this level of Ctf7-HAp expression is fully functional *in vivo* and provides for normal cell growth in otherwise *ctf7Δ* cells (9). Cells co-expressing Ctf7-HAp and Mps3Δ60–13MYCp were processed for co-immunoprecipitations as previously described with minor modifications (16). Cells were lysed by mechanical disruption and centrifuged, and extracted soluble supernatants were incubated with MYC-directed antibodies and Protein A-Sepharose beads. Protein-bead complexes were washed several times prior to Western blot analysis. Anti-MYC staining reveals that Mps3p-13MYCp is efficiently immunoprecipitated
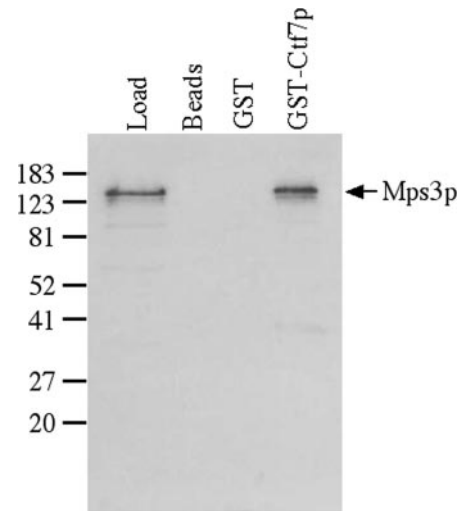
FIG. 1. **Physical association of Mps3p with Ctf7p *in vitro*.** Extracts from cells expressing Mps3-MYCp (*Load*) were used to test for Mps3p binding to the following bead matrices: glutathione-Sepharose beads (*Beads*) or beads coupled to either bacterially expressed glutathione *S*-transferase (*GST*) or GST-Ctf7p (*GST-Ctf7p*). Extract-bead complexes were washed numerous times to remove weakly bound proteins prior to eluting off specifically bound proteins. The association of Mps3p with Ctf7p was then assayed by Western blot analyses using MYC-directed antibodies. Molecular masses are shown in kDa.
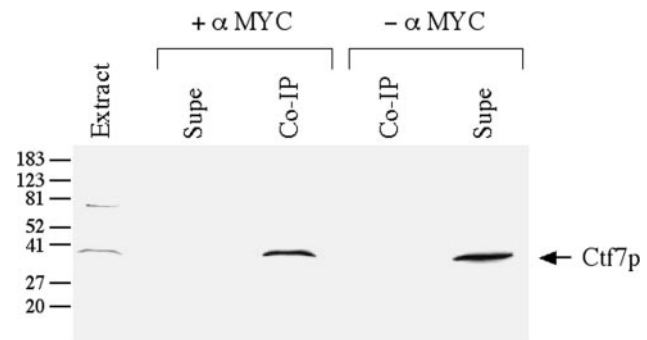

FIG. 2. **Mps3p and Ctf7p physically associate *in vivo*.** Cell lysates co-expressing Mps3-13MYCp and Ctf7-HAp were incubated with (+αMYC) or without (−αMYC) MYC-directed antibody and precipitated with Protein A-Sepharose beads. Western blot analyses of tightly bound proteins using HA-directed antibody reveals that Ctf7p is co-immunoprecipitated (*Co-IP*) with Mps3-MYCp. Co-immunoprecipitation requires the MYC-precipitating antibodies; Ctf7p remains in the supernatant (*Supe*) in the absence of MYC-directed antibodies (*αMYC*). An independently derived cell lysate sample (*Extract*) indicates Ctf7p mobility. A higher molecular weight and nonspecific protein band is sometimes detected using HA-directed antibodies, but this band fails to co-fractionate with Ctf7p. Molecular masses are shown in kDa.

under these conditions and that Mps3p immunoprecipitation requires both the MYC tag and MYC-immunoprecipitating antibody (data not shown). We then tested for the ability of Ctf7p-HA to co-immunoprecipitate with Mps3p. Parallel protein membranes containing immunoprecipitated Mps3p were probed using HA-directed antibodies. The results show that Ctf7p indeed co-immunoprecipitates with Mps3p, revealing that Ctf7p associates with Mps3p *in vivo* (Fig. 2). Importantly, Ctf7p co-immunoprecipitation with Mps3-MYCp depended on the presence of the MYC-precipitating antibody; Ctf7p remained in the supernatant and did not co-immunoprecipitate with Mps3p in the absence of the MYC-precipitating antibody (Fig. 2). In summary, the combined data obtained from two-hybrid, GST pull-down, and co-immunoprecipitation analyses reveal that Mps3p associates directly with Ctf7p.

Generation of New MPS3 Alleles—Given the physical association of Mps3p and Ctf7p, we hypothesized that Mps3p may

FIG. 3. **Characterization of new *mps3* alleles.** *A*, at 23 °C, all four *mps3* mutant strains exhibit robust growth, similar to wild type. At 37 °C, all mutant strains exhibit temperature sensitivities; *mps3-2* and *mps3-3* are tightly temperature-sensitive, whereas *mps3-4* and *mps3-5* exhibit a limited number of cell divisions prior to cell death. 10-fold dilutions for each strain culture are shown. *B*, flow cytometric DNA profiles of log growth wild type and *mps3* mutant cells at 23 °C reveal an allelic series. *mps3-2* and *mps3-4* are predominantly diploidized even at permissive temperatures (2C and 4C DNA content). In contrast, *mps3-5* cells exhibit low to moderate diploidization, and *mps3-3* cells contain a DNA content that is mostly indistinguishable from wild type cell (1C and 2C DNA content). Note that whereas *mps3-3* mutant strains contain wild type DNA contents, this allele exhibits the tightest temperature sensitivity.
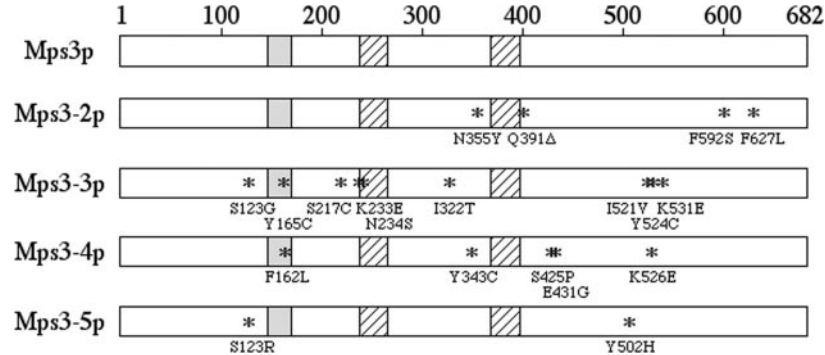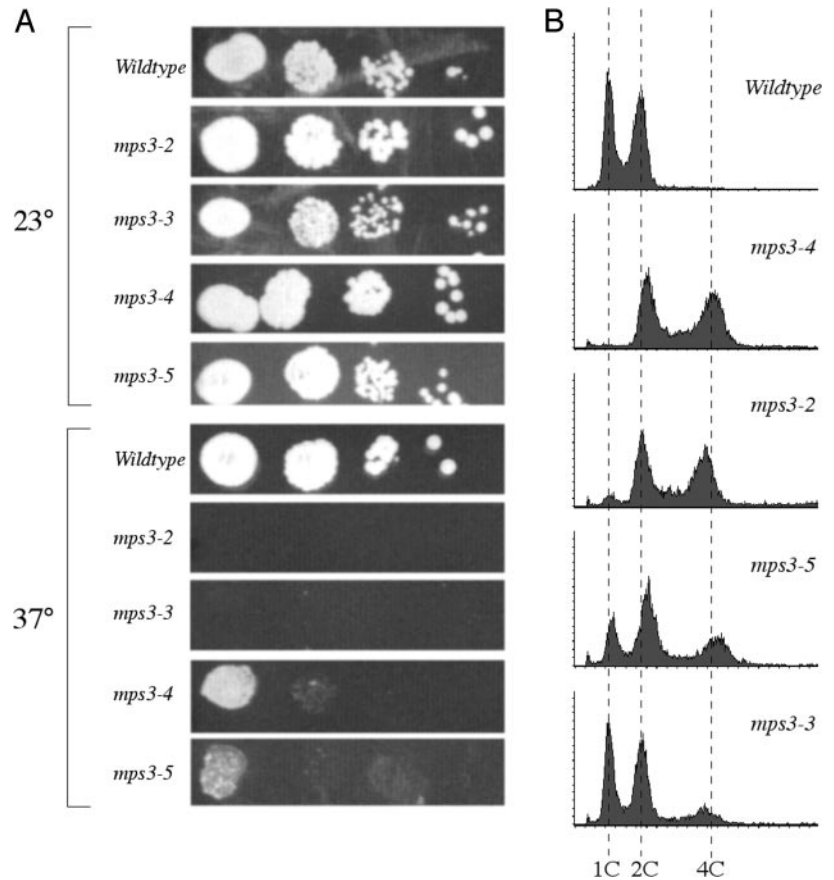
FIG. 4. **Schematic diagram (drawn to scale) summarizing sequence analyses for each new *mps3* allele.** Wild type Mps3p contains eight consecutive glutamines; thus, the glutamine in-frame deletion in Mps3-2p was arbitrarily attributed to the first glutamine (position 391). Of the two mutations in Mps3-5, one maps exactly to that found in Mps3-3, suggesting that serine 123 plays a central role in Mps3p function. The *shaded area* denotes a putative transmembrane domain, and *hatched regions* indicate predicted coiled-coil regions (3, 4). Previously described alleles do not map onto the new mutations described here: Mps3-1 = S472N (3); Nep98–7 = N597K (4).
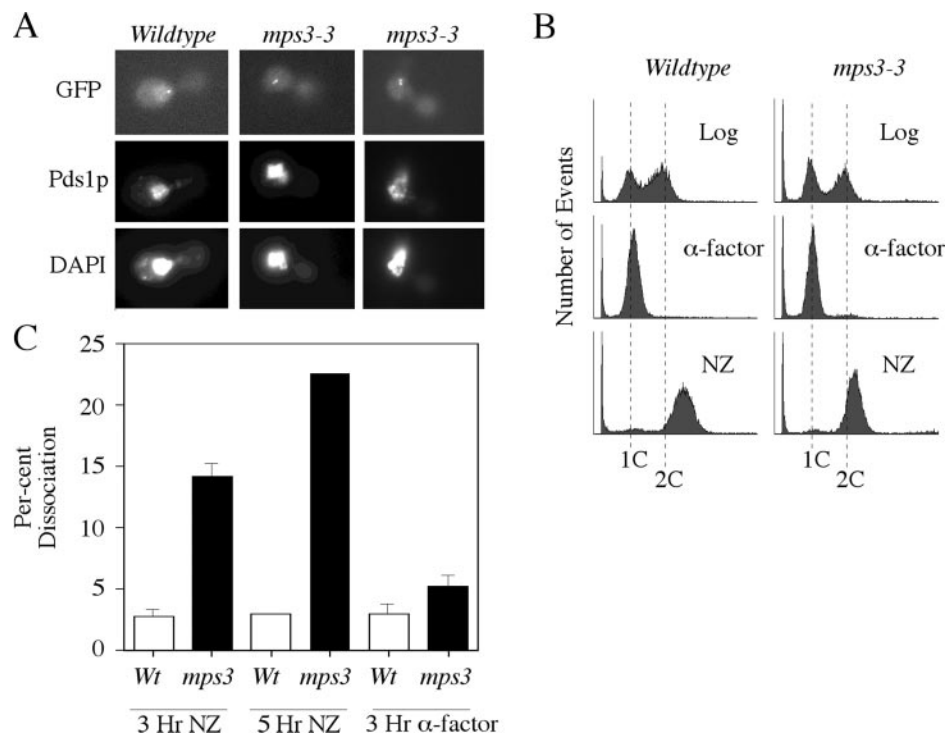
function in sister chromatid cohesion. Often, haploid cells harboring defects in spindle pole body components such as *MPS3* diploidize to produce cells with 2C and 4C DNA contents (3, 4), thereby complicating the quantification of cohesion defects. To circumvent this obstacle, we used a PCR strategy to generate conditional *mps3* alleles that exhibit wild type DNA contents (31). Briefly, *mps3Δ* cells harboring pRS316-*MPS3* were co-transformed with pooled PCR-mutagenized *MPS3* products and pRS315-*MPS3* with the majority of the *MPS3* open reading frame deleted. Of ~6000 transformants, six scored positive as temperature-sensitive after pRS316-*MPS3* counterselection (34). The four tightest temperature-sensitive alleles were stably integrated into the genome of *mps3Δ* cells, providing the only source of Mps3p function in these cells. All four mutant strains (*mps3-2*,

mps3-3, *mps3-4*, and *mps3-5*) exhibited temperature sensitivities relative to a wild type control strain (Fig. 3). DNA sequence analyses for each of these new *mps3* mutations are summarized in Fig. 4.

We tested whether these four *mps3* mutant strains exhibited a diploidization phenotype. All four strains were allowed to proceed through several cell divisions in order to accentuate the diploidization phenotype. Flow cytometry analyses of log phase wild type and *mps3* strains reveal an allelic series (Fig. 3). *mps3-2* and *mps3-4* both exhibit a completely diploidized DNA content, consistent with previously described *mps3* alleles (3, 4). In contrast, *mps3-5* mutant cells exhibit a low to intermediate level of diploidization within the cell population. *mps3-3* mutant cells exhibit predominantly wild type haploid levels of DNA that can be maintained for extended periods of

FIG. 5. **mps3 mutant strains exhibit defects in sister chromatid cohesion.** *A*, micrographs of wild type and *mps3-3* mutant strains in which sister chromatid loci (GFP) and Pds1p (Pds1p) are visualized within the DNA mass (DAPI). *B*, flow cytometric DNA profiles of wild type and *mps3* mutants strains during the experimental time course. Asynchronous log phase cultures (*Log*) of wild type and *mps3-3* mutant strains were synchronized in G_1 (α-factor) at 23 °C and released into 37 °C fresh medium containing nocodazole (*NZ*) to arrest cells prior to anaphase. *C*, quantification of cohesion defects exhibited by wild type (*MPS3*) and mutant (*mps3*) strains. 3-h time points for both nocodazole (*NZ*)- and α-factor-treated cells represent >400 cells from four independent experiments. The 5-h time point represents 100 cells counted for each strain.

time. Thus, the *mps3-3* allele provides an important tool with which to test for cohesion defects.

Mps3p Functions in Sister Chromatid Cohesion—To investigate the possibility that Mps3p might play a role in sister chromatid cohesion, *mps3-3* cells exhibiting wild type levels of DNA were crossed with a cohesion assay strain and sporulated, and appropriate spores were obtained. Diploidized cells mated to haploid cells fail to produce viable progeny. Thus, any *mps3-3* parental cells that might have diploidized prior to mating failed to contribute to the resulting progeny upon sporulation; all spores exhibited only wild type DNA contents. The cohesion assay strain contains Tet operator repeats integrated 40 kb proximal to the centromere of chromosome V and also expresses GFP-tagged Tet repressor protein, allowing for visualization of the centromere-proximal locus for each sister chromatid (14, 32). Indirect immunofluorescence further allows for nuclear detection of Pds1p, a biochemical marker of preanaphase cells (35, 36). Thus, cell morphology, GFP-tagged chromosomal loci, and coincident DNA and Pds1p staining were simultaneously assessed on a cell-by-cell basis to map the disposition of sister chromatids in preanaphase cells.

To assay for cohesion defects, log phase wild type and *mps3-3* mutant strains were synchronized in G_1 at 23 °C with α-factor and then released into 37 °C rich medium supplemented with nocodazole to arrest them in mitosis. After 3 h of incubation at 37 °C, parallel cell samples were harvested and assessed for DNA content, cell morphology, Pds1p content, and disposition of sister chromatid loci via GFP. Cell samples were harvested throughout the experimental time course to confirm that the cells remained within the first cell cycle even after 5 h post-α-factor release and had not diploidized (data not shown). Consistent with a preanaphase mitotic arrest, both wild type and *mps3-3* cells treated with nocodazole were predominantly large budded and contained a 2C DNA content (Fig. 5). Immunofluorescence analyses was used to identify large budded cells that retained Pds1p coincident with DAPI visualization. Cells confirmed as arrested prior to anaphase onset were then assessed for cohesion. Wild type cells held at 37 °C for 3 h contained tightly paired sister chromatids such that few (2.75%) sisters
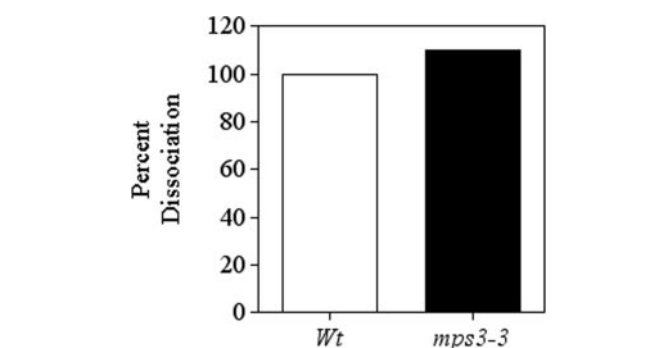
FIG. 6. **Mps3p functions in cohesion establishment and not maintenance.** Wild type and *mps3-3* mutant strains were arrested in mitosis with nocodazole prior to shifting to the restrictive temperature of 37 °C for an additional 1 h. Quantification of tightly paired sister chromatids (single GFP spots) exhibited by wild type (*Wt*) and *mps3-3* mutant (*mps3*) strains is shown as normalized to 100% of paired sisters in wild type cells. Each data point represents 200 individual cells counted from two independent experiments.

were dissociated. In contrast, *mps3-3* mutant cells contained a significant increase in the number of separated sisters (14.2%) (Fig. 5). *mps3-3* cells held for 5 h at 37 °C in nocodazole medium exhibited an even greater cohesion defect (23%), relative to identically treated wild type cells (3%). These levels of cohesion defects in *mps3* mutants are similar to those exhibited by nonessential cohesion factors (*trf4* at 20%, *chl1* at 23%, *ctf18* at 25%, *ctf8* at 30%, and *ctf18* at 35%) (12, 13, 15, 16) and reveal that Mps3p indeed functions in cohesion. To further demonstrate that the increase in the number of GFP signals was due to precocious sister separation and not aneuploidy present at the beginning of the experiment, we quantified the number of GFP signals in G_1 cells arrested with α-factor. The results show that both wild type and *mps3* strains exhibited similarly low levels (3.0 and 5.2%, respectively) of GFP signals and identical DNA profiles by fluorescence-activated cell sorting analyses, indicating that the cohesion defects observed in *mps3* preanaphase cells is not due to aneuploidy present early in the cell cycle (Fig. 5).
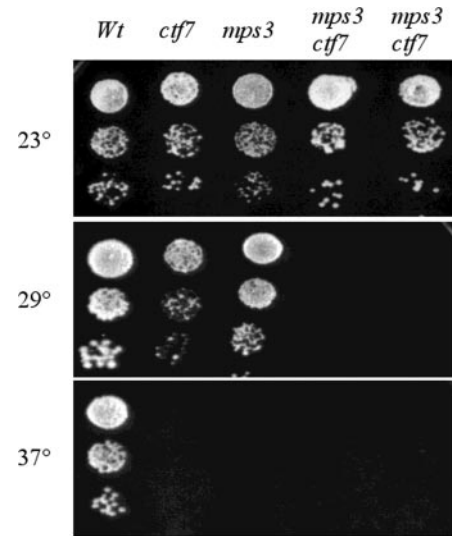
A, B panels of Fig. 7 blots
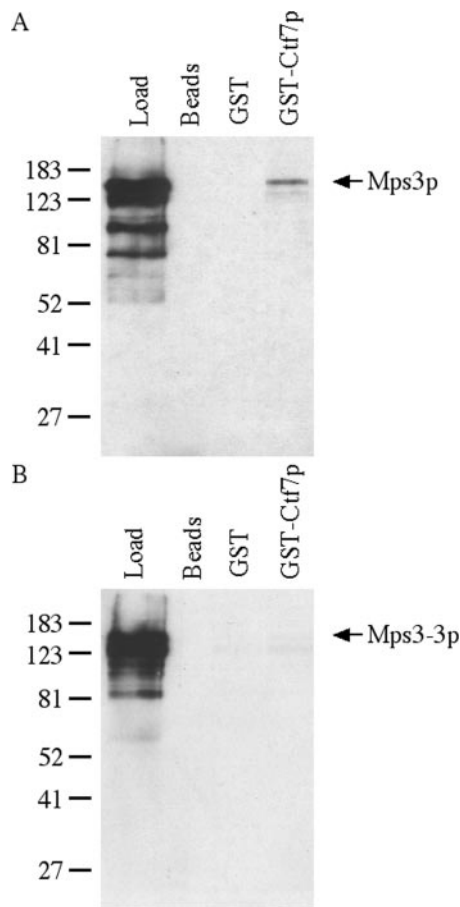
FIG. 7. **Mps3p association with Ctf7p is physiologically relevant.** *A*, Mps3-13MYCp binds to GST-Ctf7p, but not GST or beads alone, at 37 °C. *B*, Mps3-3-13MYCp fails to bind to GST-Ctf7p at 37 °C. Both Mps3-13MYCp and Mps3-3-13MYCp bind GST-Ctf7p at 23 °C (not shown). See "Results" and the legend to Fig. 2 for details.

TABLE I
Quantification of progeny obtained by crossing ctf7 and mps3 mutant strains

|	ctf7-203:LEU2, ctf7::HIS3 X mps3::KAN, mps3-3:ADE2	
	Observed	Expected
Wild type	34	30
mps3 (Kan+, Ade2+, ts)	14	15
ctf7 (Leu+, His+, ts)	15	15
ctf7, mps3	6	7
Inviable	51	53

FIG. 8. **MPS3 and CTF7 genetic interactions.** Wild type, single mutant *mps3-3* and *ctf7-203* strains, and double mutant *mps3-3 ctf7-203* strains were plated on YPD-rich medium in serial dilution and held at 23, 29, and 37 °C. All strains grew at 23 °C. Wild type and single mutant strains also grew at 29 °C. In contrast, double mutant *mps3-3 ctf7-203* strains (two of the six double mutant strains shown) failed to grow at 29 °C, revealing a conditional synthetic lethal interaction between *mps3-3* and *ctf7-203*. All mutant strains were inviable at 37 °C.

Mps3p Functions in Cohesion Establishment, Not Maintenance—Given Mps3p association with Ctf7p and role in cohesion, it became important to test whether Mps3p plays a role in cohesion maintenance or establishment. We directly tested this model using methods previously employed to reveal a role for structural cohesins in cohesion maintenance (23, 32). Briefly, log phase wild type and *mps3-3* cells were arrested in mitosis at the permissive temperature using medium supplemented with nocodazole. After 2 h, the cultures were split, and half of each culture was shifted to 37° for an additional 1 h. This regimen results in loss of cohesion for structural cohesin mutants but not establishment factors (9). As before, parallel cell samples were harvested and assessed for DNA content, cell morphology, Pds1p content, and disposition of sister chromatid loci via GFP. Despite the absence of presynchronization in G$_1$, nocodazole treatment produced predominantly mitotic cultures over this 3-h time course (wild type and *mps3-3* cultures containing 76.9 *versus* 79.9% 2C DNA contents, respectively). We normalized to 100% the frequency of wild type cells that were large budded and contained a 2C DNA content and tightly paired sisters. In comparison, *mps3-3* mutant strains treated identically exhibited a frequency of paired sister chromatids that was equal to or greater than that of wild type cells; no cohesion defect was observed (Fig. 6). These results reveal that Mps3p does not function in cohesion maintenance but instead that Mps3p participates in cohesion establishment, consistent with its association with Ctf7p.

Mps3p Association with Ctf7p Is Physiologically Relevant—Mps3p both binds Ctf7p and functions in cohesion. One predic-

tion of these findings is that *mps3-3* strains may fail in cohesion due to loss of Ctf7p-Mps3p interactions. To test this model directly, we epitope-tagged the *mps3-3* temperature allele and compared its association with Ctf7p with that of wild type Mps3p. GST-Ctf7p, GST alone, and glutathione-Sepharose beads were incubated with extracts from yeast cells expressing either Mps3-13MYCp or Mps3-3-13MYCp as described above. In this case, the binding reaction was performed for 30 min at 37 °C. Afterward, the three bead matrices were copiously washed before eluting the bound proteins. Western blot analyses of the eluted proteins confirmed again that Mps3p specifically associated with GST-Ctf7p but not with GST or beads alone (Fig. 7). In contrast, Mps3-3-13MYCp failed to bind to GST-Ctf7p at 37 °C (Fig. 7). Loss of binding was temperature-dependent such that binding reactions performed at 23 °C resulted in Mps3-3-13MYCp associating with Ctf7p (data not shown). These findings reveal that the association of Mps3p with Ctf7p is physiologically relevant; Mps3p competent to promote cohesion binds to Ctf7p, whereas Mps3-3p that is deficient in cohesion fails to associate with Ctf7p.

mps3-3 Exhibits Allele-specific Conditional Synthetic Lethality When Combined with ctf7-203—The physical association of Mps3p with Ctf7p raised the possibility that *mps3* and *ctf7* alleles also might interact genetically. To test this prediction, *mps3-3* was crossed with *ctf7-203*, and the resulting diploids were sporulated. For the *mps3-3 ctf7-203* cross, 30 of 31 tetrads produced viable spores. Of the 120 possible spores from the 30

FIG. 9. **Ctf7p does not function in spindle pole body duplication during S-phase (*left panels*) and in G$_1$ (*right panels*).** Log phase wild type and *ctf7* mutant cells arrested in either G$_1$ using α-factor or in mitosis using nocodazole were released into medium containing nocodazole and allowed to progress through the cell cycle at 37 °C to affect Ctf7p inactivation. For cells released from nocodazole, cells were allowed to progress through the cell cycle 60–90 min before the medium was supplemented with nocodazole to achieve a second cell cycle arrest. *A* and *C*, micrographs of cells stained for Tub4p (*Tub4p*) and microtubules (*MT*) and counterstained to visualize DNA (*DAPI*). Cell morphologies, as revealed by high resolution differential interference contrast (*DIC*), are also shown. *C* and *D*, quantification of monopolar spindles in wild type *versus ctf7* mutant cells. *Scale bar*, ~3.7 μm.
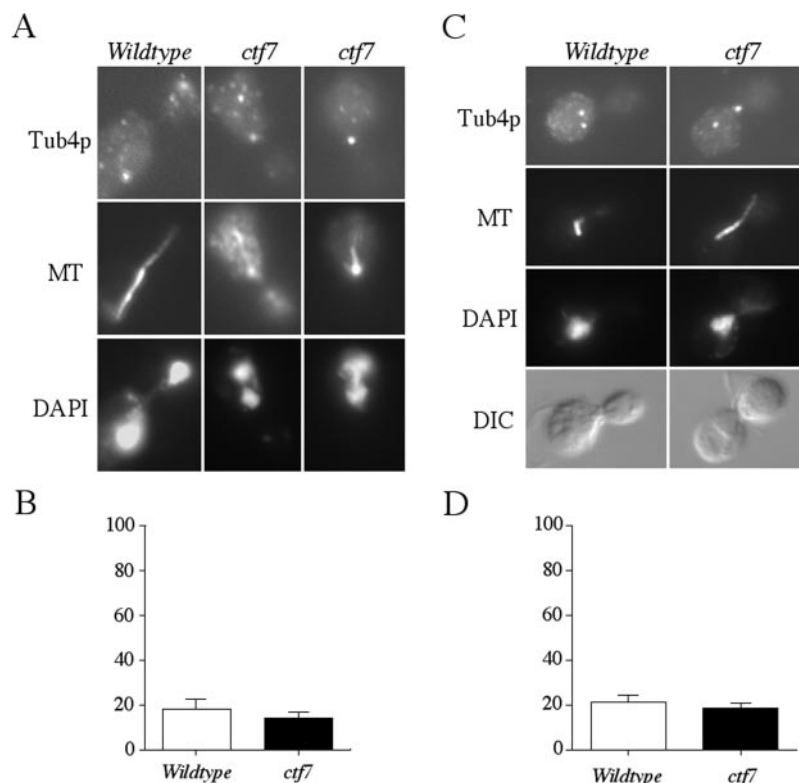
tetrads, six *mps3 ctf7* double mutant strains were obtained, nearly identical to the expected yield of seven spores (Table I). We then tested whether *mps3-3 ctf7-203* double mutant cells would exhibit growth characteristics different from strains harboring either allele alone. Importantly, all 6 *mps3-3 ctf7-203* double mutant strains exhibited a robust conditional synthetic lethal interaction. At 23 °C on YPD-rich medium, a dilution series of single mutant *mps3-3* or *ctf7-203* cells and double mutant *mps3-3 ctf7-203* cells produced dense growth plaques. At 29 °C, single mutant strains *ctf7-203* and *mps3-3* remained viable. In contrast, however, all six of the double mutant *mps3-3 ctf7-203* strains were inviable (Fig. 8). All single and double mutant strains were inviable at 37 °C. A similar interaction was not found for *mps3-5 ctf7-203* double mutants. These findings that *mps3-3* and *ctf7-203* exhibit allele-specific synthetic lethality support a model in which Mps3p and Ctf7p physically associate to perform roles in cohesion establishment.

Ctf7p Is Not Required for Spindle Pole Body Duplication—We next tested whether Ctf7p plays a role in spindle pole body duplication. Ctf7p is known to establish cohesion during S-phase (9, 21). Thus, we first tested whether S-phase Ctf7p activity was required for spindle pole body duplication. Log phase wild type and *ctf7* mutant cells were arrested in G$_1$ at 23 °C with α-factor, washed, and released in 37 °C rich medium. These cells were then allowed to proceed through the cell cycle at 37 °C, abrogating Ctf7-203p function during S-phase and G$_2$. Upon release from G$_1$, cell samples were harvested every 15 min and assayed for DNA content and cell morphology. The disposition of spindle pole bodies was determined in cell fractions in which the majority of cells were in G$_2$/M, as assayed by flow cytometry, and for cells in which the bud size was at least equal to one-half of the mother cell when viewed microscopically. To monitor for spindle pole body duplication, we visualized individual spindle poles by indirect immunofluorescence using a Tub4p-specific antibody (a generous gift from Drs. S. Jaspersen and M. Winey) (Fig. 9). Assessing spindle poles on a cell-by-cell basis, the results show that

both wild type and *ctf7* mutant cells exhibited similar low levels of monopolar spindles (Fig. 9). Occasionally, we observed that Tub4p staining was unequal between the spindle pole bodies. Thus, whereas our results probably overestimate the number of monopolar spindles in both wild type and *ctf7* mutant cells (cells in which the weaker spindle pole staining was not detected), these data support a model in which Ctf7p does not perform an essential function in spindle pole duplication during S-phase. We also tested whether Ctf7p functions in spindle pole body duplication during G$_1$. In this case, log phase wild type and *ctf7* mutant cells were arrested in preanaphase at 23 °C with nocodazole, released into rich medium held at 37 °C, and then allowed to progress through the cell cycle at 37 °C (abolishing Ctf7-203p activity through G$_1$, S-phase, and G$_2$). Quantification of Tub4p staining by immunofluorescence revealed that Ctf7p inactivation early in the cell cycle did not abrogate spindle pole duplication; both wild type and *ctf7* mutant cells exhibited similarly low levels of monopolar spindles (Fig. 9).

DISCUSSION

In this study, we used the well established cohesion establishment factor Ctf7p as a platform to identify novel cohesion proteins. Mps3p was found to interact with Ctf7p by a genome-wide two-hybrid screen. This physical interaction was confirmed both *in vivo* and *in vitro* using GST pull-down and co-immunoprecipitation strategies. The association of Ctf7p and Mps3p may not be surprising given that Ctf7p is a nuclear protein. Mps3p is a nuclear envelope protein that also associates with spindle pole body half-bridges (3, 4). Thus, Ctf7p and Mps3p may associate at the interface of the nucleoplasm and nuclear envelope especially near spindle pole bodies. Mps3p may also interact directly with chromatin components, consistent with the interactions between Ctf7p and Mps3p reported here and by previous observations that Mps3p associates with several DNA associated factors including Est1p, Hta3p, and Ndj1p (29, 37).

We used a cohesion assay strain to demonstrate that Mps3p

plays a functional role in cohesion establishment. The cohesion defect (23 *versus* 3% after 5 h and 14.2 *versus* 2.75% after 3 h of nocodazole) for *mps3* mutant cells, compared with wild type, is similar to levels exhibited by numerous nonessential cohesion factors, including *trf4* (20%), *chl1* (23%), *ctf18* (25%), *ctf8* (30%), and *ctf18* (35%) (12, 13, 15, 16). In contrast, mutations in essential cohesion factor genes, including *ctf7*, *mcd1/scc1*, *irr1/scc3*, *pds5*, *smc1*, and *smc3*, typically exhibit twice this level (50–60%) of sister separation (9, 21, 23, 32, 38–41). One interpretation of these findings is that Mps3p may play an essential role in cohesion that is redundant to other proteins, diminishing the cohesion defect observed in *mps3* alleles. Alternatively, Mps3p may perform a key but nonessential role in cohesion in addition to its essential role in spindle pole body duplication. This latter model is supported by findings that *mps3-1* mutant cells exhibit several phenotypes (including a mitotic delay) at the permissive temperature (3) and that elevated levels of Mps3p fail to rescue the essential function of Ctf7p (this study). Precedence for this model comes from studies involving Rfc5p, Rfc2p, Rfc4p, and Pol2p, which all perform essential roles in DNA replication but, when mutated, exhibit levels of cohesion loss similar to both *mps3* mutant strains and nonessential cohesion factors (10, 11, 13, 14). Our finding that a spindle pole body protein functions in cohesion is further supported by new evidence that Kar3p, a minus-end-directed spindle pole microtubule motor, participates in cohesion at levels similar to those found for Mps3p (20). Thus, our data both provide a new function for Mps3p and greatly extend a novel link between cohesion establishment and spindle pole body assembly.

Given that spindle pole body duplication and cohesion establishment both occur early in the cell cycle, it is not surprising that these fundamental chromosome segregation processes are coordinated. Formally, the physical and functional interactions between Mps3p and Ctf7p can be envisioned in numerous ways. For instance, Ctf7p may perform a dual function in both cohesion establishment and spindle pole body duplication. At the level of detection used here, however, spindle pole body duplication appears normal in *ctf7* mutant cells. Genetic assays further suggest that Ctf7p does not function in spindle pole body assembly; elevated levels of Mps3p did not rescue *ctf7* temperature sensitivity, and elevated levels of Ctf7p did not rescue *mps3* phenotypes. Another model, based on the role of Mps3p in cohesion, is that the nuclear envelope or spindle pole body serves as a staging or assembly platform for cohesion processes. In this scenario, abrogation of spindle pole body assembly coordinately results in misassembly of cohesion complexes. The identification of two spindle pole body components, Mps3p (this study) and Kar3p (20), as cohesion factors provides novel and independent lines of evidence that spindle pole body components function in cohesion.

There is strong precedence that the nuclear envelope plays a role in chromatin metabolism. For instance, perinuclear proximity is a key factor in establishing transcriptionally silent loci such as the HMR (42). The reciprocal is also true; mutations in silencing genes result in loss of both nuclear pore and nucleolar architectures (43). Recently, components required for chromatin anchorage to the nuclear envelope have been identified. Esc1p, an inner face nuclear envelope protein (along with both Ku80 and Sir4p) is required to anchor chromatin to the nuclear envelope, whereas Esc1p-dependent anchorage occurs independent of silencing (44). Furthermore, Mps1p is required for both spindle pole body duplication (including Spc42p incorporation) and mitotic checkpoint function (45–47). Consistent with these dual activities, Mps1p is located at both the spindle pole and kinetochores. Similar kinetochore/spindle pole body

co-localization has been reported for Mad2p, anaphase-promoting complex subunits, and a host of centromere-binding proteins (8, 48). In parallel, numerous nuclear pore proteins now appear to associate with kinetochores in both yeast and mammalian cells and function in transcriptional repression (49–51). The functional interaction between Ctf7p and Mps3p reported here suggests that spindle pole body proteins play an additional and key role in coordinating assembly reactions required for establishing sister chromatid cohesion.

REFERENCES

1. Winey, M., and O'Toole, E. T. (2001) *Nat. Cell Biol.* **3,** E23–E27
2. Adams, I. R., and Kilmartin, J. V. (2000) *Trends Cell Biol.* **10,** 329–335
3. Jaspersen, S. L., Giddings, T. H., Jr., and Winey, M. (2002) *J. Cell Biol.* **159,** 945–956
4. Nishikawa, S., Terazawa, Y., Nakayama, T., Hirata, A., Makio, T., and Endo, T. (2003) *J. Biol. Chem.* **278,** 9938–9943
5. Francis, S. E., and Davis, T.N. (2000) *Curr. Top. Dev. Biol.* **49,** 105–132
6. Koshland, D. E., and Guacci, V. (2000) *Curr. Opin. Cell Biol.* **12,** 297–301
7. Nasmyth, K., Peters, J. M., and Uhlmann, F. (2000) *Science* **288,** 1379–1385
8. Skibbens, R. V. (2000) *Genome Res.* **10,** 1664–1671
9. Skibbens, R. V., Corson, L. B., Koshland, D., and Hieter, P. (1999) *Genes Dev.* **13,** 307–319
10. Krause, S. A., Loupart, M. L., Vass, S., Schoenfelder, S., Harrison, S., and Heck, M. M. (2001) *Mol. Cell. Biol.* **21,** 5156–5168
11. Edwards, S., Li, C.M., Levy, D.L., Brown, J., Snow, P.M., and Campbell, J. (2003) *Mol. Cell. Biol.* **23,** 2733–2748
12. Hanna, J. S., Kroll, E. S., Lundblad, V., and Spencer, F. A. (2001) *Mol. Cell. Biol.* **21,** 3144–3158
13. Mayer, M. L., Gygi, S. P., Aebersold, R., and Hieter, P. (2001) *Mol. Cell* **7,** 959–970
14. Kenna, M. A., and Skibbens, R. V. (2003) *Mol. Cell. Biol.* **23,** 2999–3007
15. Wang, Z., Castano, I. B., De Las Penas, A., Adams, C., and Christman, M. F. (2000) *Science* **289,** 774–779
16. Skibbens, R. V. (2004) *Genetics* **166,** 32–44
17. Nasmyth, K. (2001) *Annu. Rev. Genet.* **35,** 673–745
18. Cohen-Fix, O. (2001) *Cell* **106,** 137–140
19. Warren, C. D., Eckley, D. M., Lee, M. S., Hanna, J. S., Hughes, A., Peyser, B., Jie, C., Irizarry, R., and Spencer, F. A. (2004) *Mol. Biol. Cell* **15,** 1724–1735
20. Mayer, M. L., Pot, I., Chang, M., Xu, H., Aneuliunas, V., Kowk, T., Newitt, R., Aebersold, R., Boone, C., Brown, G.W., and Hieter, P. (2004) *Mol. Biol. Cell* **15,** 1736–1745
21. Toth, A., Ciosk, R., Uhlmann, F., Galova, M., Schleiffer, A., and Nasmyth, K. (1999) *Genes Dev.* **13,** 320–333
22. Ciosk, R., Shirayama, M., Shevchenko, A., Tanaka, T., Toth, A., Shevchenko, A., and Nasmth, K. (2000) *Mol. Cell* **5,** 243–254
23. Guacci, V., Koshland, D., and Strunnikov, A. (1997) *Cell* **91,** 47–57
24. Deming, P. B., Cistulli, C. A., Zhao, H., Graves, P. R., Piwnica-Worms, H., Paules, R. S., Downes, C. S., and Kaufmann, W. K. (2001) *Proc. Natl. Acad. Science* **98,** 12044–12049
25. Venkitaraman, A. R. (2002) *Cell* **108,** 171–182
26. Brosh, R. M., and Bohr, V. A. (2002) *Exp. Gerontol.* **37,** 491–506
27. Thompson, L. H., and Schild, D. (2002) *Mutat. Res.* **509,** 49–78
28. James, P., Halladay, J., and Craig, E. A. (1996) *Genetics* **144,** 1425–1436
29. Uetz, P., Giot, L., Cagney, G., Mansfield, T. A., Judson, R. S., Knight, J. R., Lockshon, D., Narayan, V., Srinivasan, M., Pochart, P., Qureshi-Emili, A., Li, Y., Godwin, B., Conover, D., Kalbfleisch, T., Vijayadamodar, G., Yang, M., Johnston, M., Fields, S., and Rothberg, J. M. (2000) *Nature* **403,** 623–627
30. Boeke, J. D., Trueheart, J., Natsoulis, G., and Fink, G. R. (1987) *Methods Enzymol.* **154,** 164–175
31. Kassenbrock, C. K., Cao, W., and Douglas, M. G. (1993) *EMBO J.* **12,** 3023–3034
32. Michaelis, C., Ciosk, R., and Nasmyth, K. (1997) *Cell* **91,** 35–45
33. Bellows, A. M., Kenna, M.A., Cassimeris, L., and Skibbens, R.V. (2003) *Nucleic Acids Res.* **31,** 6334–6343
34. Boeke, J. D., LaCroute, F., and Fink, G. R. (1984) *Mol. Gen. Genet.* **197,** 345–346
35. Yamamoto, A., Guacci, V., and Koshland, D. (1996) *J. Cell Biol.* **133,** 99–110
36. Cohen-Fix, O., Peters, J. M., Kirschner, M. W., and Koshland, D. (1996) *Genes Dev.* **10,** 3081–3093
37. Ito, T., Chiba, T., Ozawa, R., Yoshida, M., Hattori, M., and Sakaki, Y. (2001) *Proc. Natl. Acad. Sci. U. S. A.* **98,** 4569–4574
38. Strunnikov, A. V., Larionov, V. L., and Koshland, D. (1993) *J. Cell Biol.* **123,** 1635–1648
39. Kurlandzka, A., Rytka, J., Gromadka, R., and Murawski, M. (1995) *Yeast* **11,** 885–890
40. Hartman, T., Stead, K., Koshland, D., and Guacci, V. (2000) *J. Cell Biol.* **151,** 613–626
41. Panizza, S., Tanaka, T., Hochwagen, A., Eisenhaber, F., and Nasmyth, K. (2000) *Curr. Biol.* **10,** 1557–1564
42. Andrulis, E. D., Neiman, A.M., Zappulla, D.C., and Sternglanz, R. (1998) *Nature* **394,** 592–595
43. Teixeira, M. T., Dujon, B., and Fabre, E. (2002) *J. Mol. Biol.* **321,** 551–561

44. Taddei, A., Hediger, F., Neumann, F. R., Bauer, C., and Gasser, S. M. (2004) *EMBO J.* **23,** 1301–1312
45. Weiss, E., and Winey, M. (1996) *J. Cell Biol.* **132,** 111–123
46. Winey, M., Goetsch, L., Baum, P., and Byers, B. (1991) *J. Cell Biol.* **114,** 745–754
47. Castillo, A. R., Meehl, J.B., Morgan, G. Schutz-Geschwender, A., and Winey, M. (2002) *J. Cell Biol.* **156,** 453–465
48. Cassimeris, L., and Skibbens, R. V. (2003) *Curr. Issues Mol. Biol.* **5,** 99–112
49. Belgareh, N., Rabut, G., Bai, S.W., van Overbeek, M., Beaudouin, J., Daigle, N., Zatsepina, O. V., Pasteau, F., Labas, V., Fromont-Racine, M., Ellenberg, J., and Doye, V. (2001) *J. Cell Biol.* **154,** 1147–1160
50. Iouk, T., Kerscher, O., Scott, R. J., Basrai, M. A., and Wozniak, R. W. (2002) *J. Cell Biol.* **159,** 807–819
51. Salina, D., Enarson, P., Rattner, J. B., and Burke, B. (2003) *J. Cell Biol.* **162,** 991–1001